An Equivariant Approach to Robust State Estimation for the ArduPilot Autopilot System

Alessandro Fornasier[1], Yixiao Ge[2], Pieter van Goor[2], Martin Scheiber[1], Andrew Tridgell[2], Robert Mahony[2] and Stephan Weiss[1]

***Abstract*—The majority of commercial and open-source autopilot software for uncrewed aerial vehicles rely on the tried and tested extended Kalman filter (EKF) to provide the state estimation solution for the inertial navigation system (INS). While modern implementations achieve remarkable robustness, it is often due to the careful implementation of exception code for a multitude of corner cases along with significant skilled tuning effort. In this paper, we use the data wealth of the ArduPilot community to identify and highlight the most common real-world challenges in INS state estimation, including sensor self-calibration, robustness in static conditions, global navigation satellite system (GNSS) outliers and shifts, and robustness to faulty inertial measurement units (IMUs). We propose a novel equivariant filter (EqF) formulation for the INS solution that exploits a Semi-Direct-Bias symmetry group for multi-sensor fusion with self-calibration capabilities and incorporates equivariant velocity-type measurements. We augment the filter with a simple innovation-covariance inflation strategy that seamlessly handles GNSS outliers and shifts without requiring coding of a whole set of exception cases. We use real-world data from the Ardupilot community to demonstrate the performance of the proposed filter on known cases where existing filters fail without careful exception handling or case-specific tuning and benchmark against the ArduPilot's EKF3, the most sophisticated EKF implementation currently available.**

I. Introduction

The simple formulation and its computationally efficient implementation have made the extended Kalman filter (EKF) and its derivates the dominant state estimator for applications in robotics and on uncrewed aerial vehicles (UAVs). Over the years, sophisticated approaches have been developed to tackle their limitations. Suboptimal linearization properties can be tackled by using the unscented Kalman filter formulation [1], challenges related to discretization and observability can be managed by utilizing first-estimate Jacobians [2] and observability constrained techniques [3], high computational complexity is tackled by careful management of state dimension [4], and difficulties in effectively extracting information can be tackled by the design of information-rich trajectories [5]. Despite these extensions, EKF-based state estimators remain fragile to unmodelled noise and model uncertainty and continue to have a non-negligible failure rate under real world conditions. With community-driven EKF-based autopilot systems such as PX4 [6] and ArduPilot [7] gaining interest due to their open-source nature, versatility, and widespread adoption, there is an increasing demand of reliable and accurate estimation capabilities. The vast amount of flight tests and failure data available to these communities has led to highly sophisticated failure mitigation modules that handle corner failure cases for EKF formulations in PX4 and ArduPilot. Indeed, ArduPilot's EKF3, including all its safety modules, health monitors, and verification routines, is arguably the most sophisticated and robust EKF-based estimator available for real-world UAVs.

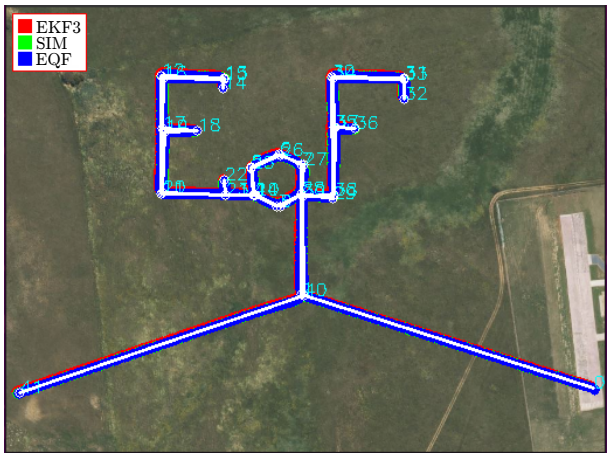

Figure 1. EqF shape simulated flight. In blue is the estimated path from the proposed EqF, in red is the estimated path from the ArduPilot internal estimator EKF3, and in green is the ground truth trajectory.

Geometry-based estimators, such as the recently published invariant extended Kalman filter (IEKF) [8] and equivariant filter (EqF) [9], provide promising results in terms of improved estimator consistency, convergence rate, and basin of convergence without requiring the same suite of health and safety modules as the multiplicative extended Kalman filter (MEKF) [10] and classical EKF algorithms. The unified geometric description of navigation and bias states [11], [12], [13], for the EqF formulation, ensure additional benefits, particularly in the transients [12], [13]. The published results on these filters, however, are still research implementations without several of critical real-world modules. Adding elements such as sensor extrinsic calibration and velocity measurements

[1]Alessandro Fornasier, Martin Scheiber, and Stephan Weiss are with the Control of Networked Systems Group, University of Klagenfurt, Austria. {name.surname}@ieee.org

[2]Yixiao Ge, Pieter van Goor, Andrew Tridgell, and Robert Mahony are with the System Theory and Robotics Lab, Australian National University, Australia. {name.surname}@anu.edu.au

This work was supported in part by the European Union's Horizon 2020 research and innovation program under grant agreement 871260 (BugWright2), in part by the Australian Research Council through the Discovery Project under Grant DP210102607, and in part by the Australian government research training program (AGRTP).

Pre-print version, accepted to ICRA24 in Jan/2024, ©IEEE.
DOI: 10.1109/ICRA57147.2024.10611108

(doppler GNSS) are of paramount importance for state-of-the-art open source code but requires finding new symmetries for the problem at hand, which is not as trivial as for the EKF.

In this paper, we propose an EqF that incorporates all the usual sensor measurements (IMUs, magnetometers, GNSS position and velocity) and that is capable of online sensor self-calibration, aiming at enhancing the system's robustness and accuracy in real-world situations. The design is based on a semi-direct product symmetry that integrates bias states into the geometric framework and avoids over-parametrisation of the state. The symmetry is extended from previous work [13], [14] to include calibration states and velocity measurements. We conduct experimental evaluation of the proposed filter in the Ardupilot software in the loop (SITL) environment, as well as evaluating on real-world flight data from multicopter platforms to validate the effectiveness and reliability of the proposed approach. Furthermore, we leverage the wealth of data available to the ArduPilot community to identify a suite of real-world scenarios that are challenging for currently established estimators. These sequences include online sensor self-calibration; robustness to prolonged static conditions such as the case of an aircraft waiting for takeoff; GNSS outliers, commonly referred to as glitches; as well as sudden changes in the GNSS solution due to a different satellite constellation or as environmental occlusions diminish, commonly referred as GNSS shifts; and robustness to noisy and faulty IMU experiencing high vibrations, or aliasing. The proposed filter is inherently robust to most of these difficulties, and along with a single simple and highly robust uncertain observation handling strategy to process output measurements, we are able to achieve state-of-the-art performance across these challenging scenarios without case-specific tuning and the suite of code to manage corner cases and exceptions. Our motivation is to develop a state estimation algorithm for an INS solution targeted at small-scale robotic systems that does not require expert knowledge to tune and is robust to the wide variety of real-world failure scenarios that real systems encounter.

The main contributions of the paper are:

- A novel equivariant filter formulation extending the previously introduced Semi-Direct-Bias symmetry group [13] to *encompass extrinsic calibration states of sensors*, including lever arm calibration for GNSS receivers and rotational calibration for magnetometers.
- Incorporation of velocity-type measurements within the equivariant filter *achieving third-order linearization error of the output map through equivariance*, enhancing the overall accuracy of the estimation.
- Application of an innovation-covariance inflation technique to *handle uncertain observations and measurement outages* across different scenarios based on the concept of generalized covariance union (GCU) [15], [16] with a flexible convergence rate.

Experiments are conducted under challenging scenarios using both simulated data in software in the loop environment and real-world flight data from diverse platforms. The evaluations focus on the behavior of the proposed EqF, using the same fixed tuning parameters throughout all tests in this paper to demonstrate its insensitivity to (expert-)tuning.

II. Notation and Mathematical Preliminaries

In this paper, we use the following notation. Bold lowercase letters are used to indicate vector quantities. Bold capital letters are used to indicate matrices. Regular letters are used to indicate elements of a manifold or a symmetry group.

Frames of reference are denoted as $\{A\}$ and $\{B\}$. A vector encoding the translation between a frame of reference $\{A\}$ and a frame of reference $\{B\}$ expressed the in frame of reference $\{A\}$ is denoted ${}^{A}\boldsymbol{p}_{B}$. Similarly, a vector encoding the relative velocity of a moving frame of reference $\{B\}$ expressed in a frame of reference $\{A\}$ are denoted by ${}^{A}\boldsymbol{v}_{B}$. In general, vectors describing physical quantities expressed in a frame of reference $\{A\}$ are denoted by ${}^{A}\boldsymbol{x}$. Rotation matrices encoding the orientation of a frame of reference $\{B\}$ with respect to a reference $\{A\}$ are denoted by ${}^{A}\mathbf{R}_{B}$; in particular, ${}^{A}\mathbf{R}_{B}$ expresses a vector ${}^{B}\boldsymbol{x}$ defined in the $\{B\}$ frame of reference into a vector ${}^{A}\boldsymbol{x} = {}^{A}\mathbf{R}_{B}\,{}^{B}\boldsymbol{x}$ expressed in the $\{A\}$ frame of reference. Finally, $\mathbf{I}_n \in \mathbb{R}^{n\times n}$ is the $n \times n$ identity matrix, and $\mathbf{0}_{n\times m} \in \mathbb{R}^{n\times m}$ is the $n \times m$ zero matrix.

Let $\mathbf{G}$ be a Lie group, and $\mathfrak{g}$ its Lie algebra. The Lie algebra $\mathfrak{g}$ is isomorphic to a vector space $\mathbb{R}^n$ of dimension $n = \dim(\mathfrak{g})$. Define the *wedge* map and its inverse, the *vee* map, as linear mappings between the vector space and the Lie algebra

$$(\cdot)^{\wedge} : \mathbb{R}^n \to \mathfrak{g},$$
$$(\cdot)^{\vee} : \mathfrak{g} \to \mathbb{R}^n.$$

Define the *Adjoint matrix* for the group, and the *adjoint matrix* for the algebra, to be, respectively the maps

$$\mathbf{Ad}_X^{\vee} : \mathbb{R}^n \to \mathbb{R}^n,$$
$$\mathbf{ad}_{\boldsymbol{u}}^{\vee} : \mathbb{R}^n \to \mathbb{R}^n,$$

for every $X \in \mathbf{G}$ and $\boldsymbol{u}^{\wedge}, \boldsymbol{v}^{\wedge} \in \mathfrak{g}$. The two adjoint matrices commute in the sense that

$$\mathbf{Ad}_X^{\vee}\mathbf{ad}_{\boldsymbol{u}}^{\vee} = \mathbf{ad}_{\mathbf{Ad}_X^{\vee}\boldsymbol{u}}^{\vee}\mathbf{Ad}_X^{\vee}.$$

For all $\boldsymbol{a}, \boldsymbol{b}, \boldsymbol{c} \in \mathbb{R}^3 \mid (\boldsymbol{a}, \boldsymbol{b}, \boldsymbol{c}) \in \mathbb{R}^9$, define the maps

$$\Pi(\cdot) : \mathfrak{se}_2(3) \to \mathfrak{se}(3), \quad \Pi\left((\boldsymbol{a}, \boldsymbol{b}, \boldsymbol{c})^{\wedge}\right) = (\boldsymbol{a}, \boldsymbol{b})^{\wedge} \in \mathfrak{se}(3).$$

For all $X = (A, a, b) \in \mathbf{SE}_2(3) \mid A \in \mathbf{SO}(3), a, b \in \mathbb{R}^3$, define the maps

$$\Gamma(\cdot) : \mathbf{SE}_2(3) \to \mathbf{SO}(3), \quad \Gamma(X) = A \in \mathbf{SO}(3),$$
$$\chi(\cdot) : \mathbf{SE}_2(3) \to \mathbf{SE}(3), \quad \chi(X) = (A, a) \in \mathbf{SE}(3).$$

III. The Biased Inertial Navigation Problem

Consider a UAV receiving angular velocity and acceleration measurements from an IMU, as well as measurements from a GNSS receiver and measurements of the magnetic north direction from a magnetometer. We will refer to the global inertial frame of reference as $\{G\}$, the frame of reference

associated with the IMU as $\{I\}$, and the frame of reference associated with the magnetometer as $\{M\}$. Let ${}^{G}\mathbf{R}_{I}$ denote the rigid body orientation, and ${}^{G}\boldsymbol{p}_{I}$ and ${}^{G}\boldsymbol{v}_{I}$ denote the rigid body position and velocity expressed in the $\{G\}$ frame, respectively. The gravity vector ${}^{G}\boldsymbol{g}$ is expressed in frame $\{G\}$. The gyroscope measurement and bias are written ${}^{I}\boldsymbol{\omega}$ and ${}^{I}\boldsymbol{b}_{\boldsymbol{\omega}}$. The accelerometer measurement and bias are written ${}^{I}\boldsymbol{a}$ and ${}^{I}\boldsymbol{b}_{\boldsymbol{a}}$. The rotational calibration of the magnetometer is denoted as ${}^{I}\mathbf{R}_{M}$, whereas the GNSS sensor lever arm is denoted as ${}^{I}\boldsymbol{t}$. Assuming a non-rotating, flat Earth scenario, the deterministic (noise-free) continuous-time system is defined as follows.

$$
\begin{aligned}
{}^{G}\dot{\mathbf{R}}_{I} &= {}^{G}\mathbf{R}_{I}\left({}^{I}\boldsymbol{\omega} - {}^{I}\boldsymbol{b}_{\boldsymbol{\omega}}\right)^{\wedge}, && \text{(1a)} & {}^{I}\dot{\boldsymbol{b}}_{\boldsymbol{\omega}} &= \mathbf{0}_{3\times1}, && \text{(1e)}\\
{}^{G}\dot{\boldsymbol{v}}_{I} &= {}^{G}\mathbf{R}_{I}\left({}^{I}\boldsymbol{a} - {}^{I}\boldsymbol{b}_{a}\right) + {}^{G}\boldsymbol{g}, && \text{(1b)} & {}^{I}\dot{\boldsymbol{b}}_{\boldsymbol{a}} &= \mathbf{0}_{3\times1}, && \text{(1f)}\\
{}^{G}\dot{\boldsymbol{p}}_{I} &= {}^{G}\boldsymbol{v}_{I}, && \text{(1c)} & {}^{I}\dot{\boldsymbol{t}} &= \mathbf{0}_{3\times1}, && \text{(1g)}\\
{}^{I}\dot{\mathbf{R}}_{M} &= \mathbf{0}^{\wedge}_{3\times1}. && \text{(1d)}
\end{aligned}
$$

The state space of the biased inertial navigation systems is $\mathcal{M} = \mathcal{SO}(3)\times\mathbb{R}^3\times\mathbb{R}^3\times\mathbb{R}^3\times\mathbb{R}^3\times\mathbb{R}^3\times\mathcal{SO}(3)$ where the five copies of $\mathbb{R}^3$ model velocity, position, and angular velocity and acceleration bias, and the GNSS sensor lever arm respectively, and $\mathcal{SO}(3)$ is the $\mathbf{SO}(3)$-torsor with rotation matrices representing coordinates of orientation rather than physical rotation of space. An element ξ of the system's state, and an element u of the input space are written

$$
\begin{aligned}
\xi &= \left({}^{G}\mathbf{R}_{I}, {}^{G}\boldsymbol{v}_{I}, {}^{G}\boldsymbol{p}_{I}, {}^{I}\boldsymbol{b}_{\boldsymbol{\omega}}, {}^{I}\boldsymbol{b}_{\boldsymbol{a}}, {}^{I}\boldsymbol{t}, {}^{I}\mathbf{R}_{M}\right) \in \mathcal{M},\\
u &= \left({}^{I}\boldsymbol{\omega}, {}^{I}\boldsymbol{a}, \mathbf{0}_{3\times1}, \mathbf{0}_{3\times1}, \mathbf{0}_{3\times1}, \mathbf{0}_{3\times1}\right) \in \mathbb{L} \subset \mathbb{R}^{18}.
\end{aligned}
$$

We now define the three measurement models considered in this work. Firstly, consider the case where measurements of the known magnetic north direction ${}^{G}\boldsymbol{m}$ are received in the magnetometer frame ${}^{M}\boldsymbol{m}$. The output space associated with such measurements is $\mathcal{N} \coloneqq \mathbb{S}^2$, and the configuration output $h_m : \mathcal{M} \to \mathcal{N}_m$ is given by

$$
h_m(\xi) = {}^{I}\mathbf{R}_{M}^{\top}\,{}^{G}\mathbf{R}_{I}^{\top}\,{}^{G}\boldsymbol{m} \in \mathcal{N}_m. \tag{2}
$$

Secondly, consider the case where position measurements ${}^{G}\boldsymbol{\pi} = {}^{G}\boldsymbol{p}_{I} + {}^{G}\mathbf{R}_{I}\,{}^{I}\boldsymbol{t}$, are received from a GNSS receiver. The associated output space is $\mathcal{N}_p \coloneqq \mathbb{R}^3$, and, to benefit from the equivariance, the configuration output $h_p : \mathcal{M} \to \mathcal{N}_p$ is defined according to [13]

$$
h_p(\xi) = {}^{G}\mathbf{R}_{I}^{\top}\left({}^{G}\boldsymbol{\pi} - \left({}^{G}\boldsymbol{p}_{I} + {}^{G}\mathbf{R}_{I}\,{}^{I}\boldsymbol{t}\right)\right) \in \mathcal{N}_p. \tag{3}
$$

Finally, consider the case where velocity measurements ${}^{G}\boldsymbol{\nu} = {}^{G}\boldsymbol{v}_{I} + {}^{G}\mathbf{R}_{I}\,{}^{I}\boldsymbol{\omega}^{\wedge}\,{}^{I}\boldsymbol{t}$, are received from a GNSS receiver. The associated output space is $\mathcal{N}_v \coloneqq \mathbb{R}^3$. To achieve third-order linearization error of the output map through equivariance, we propose the idea of extending the configuration output in Equ. (3) to the velocity measurements. Thus, we define the configuration output $h_v : \mathcal{M} \to \mathcal{N}_v$ as

$$
h_v(\xi) = {}^{G}\mathbf{R}_{I}^{\top}\left({}^{G}\boldsymbol{\nu} - \left({}^{G}\boldsymbol{v}_{I} + {}^{G}\mathbf{R}_{I}\,{}^{I}\boldsymbol{\omega}^{\wedge}\,{}^{I}\boldsymbol{t}\right)\right) \in \mathcal{N}_v. \tag{4}
$$

In the latter two measurement models, position and velocity measurements are reformulated by constructing the vectors $\boldsymbol{\pi}$, and $\boldsymbol{\nu}$ with raw position and velocity measurements respectively, and assuming $h_p(\xi) = h_v(\xi) = \mathbf{0}_{3\times1}$. More details on the fundamental derivations for the position measurements are provided in our prior work [13].

Table I
SYMMETRY GROUP ELEMENTS

(C,γ)	$\mathbf{SE}_2(3)\ltimes\mathfrak{se}(3)$	$A = \Gamma(C)$	$\mathbf{SO}(3)$
δ	$\mathbb{R}^3$	$B = \chi(C)$	$\mathbf{SE}(3)$
E	$\mathbf{SO}(3)$		

Table II
SYMMETRY GROUP INVERSE AND GROUP PRODUCT

XY	$\left(C_X C_Y, \gamma_X + \mathrm{Ad}_{C_X}[\gamma_Y], \delta_X + A_X\delta_Y, E_X E_Y\right)$
X^{-1}	$\left(C^{-1}, -\mathrm{Ad}_{B^{-1}}[\gamma], -A^{\top}\delta, E^{\top}\right)$

Table III
SYMMETRY GROUP ACTIONS

$\phi : \mathbf{G}\times\mathcal{M} \to \mathcal{M}$	$\left(\mathbf{T}C, \mathbf{Ad}^{\vee}_{B^{-1}}(\boldsymbol{b} - \gamma^{\vee}), A^{\top}(\boldsymbol{t} - \delta), A^{\top}\mathbf{S}E\right)$
$\rho_m : \mathbf{G}\times\mathcal{N}_m \to \mathcal{N}_m$	$E^{\top}y_m$
$\rho_p : \mathbf{G}\times\mathcal{N}_p \to \mathcal{N}_p$	$A^{\top}(y_p - b + \delta)$
$\rho_v : \mathbf{G}\times\mathcal{N}_v \to \mathcal{N}_v$	$A^{\top}\left(y_v - a - \delta^{\wedge}\,{}^{I}\boldsymbol{\omega}\right)$

IV. INS SYMMETRY

In the following section, we quickly recall the Semi-Direct-Bias symmetry $\mathbf{G}_{\mathbf{SD}}$ of the biased inertial navigation system introduced in our previous work [13] and extend it to include the calibration states of the sensors suite considered in this work.

Let $\mathbf{T} = \left({}^{G}\mathbf{R}_{I}, {}^{G}\boldsymbol{v}_{I}, {}^{G}\boldsymbol{p}_{I}\right)$ denotes the extended pose of the system [8], and $\boldsymbol{b} = \left({}^{I}\boldsymbol{b}_{\boldsymbol{\omega}}, {}^{I}\boldsymbol{b}_{\boldsymbol{a}}\right)$ denotes the IMU biases. Let $\mathbf{S} = {}^{I}\mathbf{R}_{M}$, and $\boldsymbol{t} = {}^{I}\boldsymbol{t}$ denote the calibration states of the magnetometer and GNSS antenna respectively. Define the matrices

$$
\begin{aligned}
\mathbf{G} &= \left(\mathbf{0}_{3\times1}, {}^{G}\boldsymbol{g}, \mathbf{0}_{3\times1}\right)^{\wedge} \in \mathfrak{se}_2(3) \subset \mathbb{R}^{5\times5},\\
\mathbf{B} &= \left({}^{I}\boldsymbol{b}_{\boldsymbol{\omega}}, {}^{I}\boldsymbol{b}_{\boldsymbol{a}}, \mathbf{0}_{3\times1}\right)^{\wedge} \in \mathfrak{se}_2(3) \subset \mathbb{R}^{5\times5},\\
\mathbf{W} &= \left({}^{I}\boldsymbol{\omega}, {}^{I}\boldsymbol{a}, \mathbf{0}_{3\times1}\right)^{\wedge} \in \mathfrak{se}_2(3) \subset \mathbb{R}^{5\times5},\\
\mathbf{N} &= \begin{bmatrix} \mathbf{0}_{3\times3} & \mathbf{0}_{3\times1} & \mathbf{0}_{3\times1} \\ \mathbf{0}_{1\times3} & 0 & 1 \\ \mathbf{0}_{1\times3} & 0 & 0 \end{bmatrix} \in \mathbb{R}^{5\times5}.
\end{aligned}
$$

The first three equations of the system in Equ. (1) can then be written in a compact way as follows [13]

$$
\dot{\mathbf{T}} = \mathbf{T}\left(\mathbf{W} - \mathbf{B} + \mathbf{N}\right) + \left(\mathbf{G} - \mathbf{N}\right)\mathbf{T}, \tag{5}
$$

Let $X, Y \in \mathbf{G}$ be two elements of the symmetry group $\mathbf{G} \coloneqq (\mathbf{SE}_2(3)\ltimes\mathfrak{se}(3))\ltimes\mathbb{R}^3\times\mathbf{SO}(3)$, whose elements are defined as in Tab. I, then the group product and the group inverse are defined as in Tab. II. Note that A, B in Tab. I are sub-elements of C computed through the maps defined in

Sec. II. Actions of the symmetry group on the state space and output space are defined in Tab. III, where $y_m \in \mathcal{N}_m$, $y_p \in \mathcal{N}_p$ and $y_v \in \mathcal{N}_v$

The existence of a transitive group action of the symmetry group $\mathbf{G}$ on the state space $\mathcal{M}$ guarantees the existence of a lift [17] $\Lambda : \mathcal{M} \times \mathbb{L} \to \mathfrak{g}$.

Theorem 4.1. *Define the lift $\Lambda(\xi, u)$ with the four maps $\Lambda_1(\xi, u), \Lambda_2(\xi, u), \Lambda_3(\xi, u), \Lambda_4(\xi, u)$ as follows*

$$\Lambda_1(\xi, u) \coloneqq (\mathbf{W} - \mathbf{B} + \mathbf{N}) + \mathbf{T}^{-1}(\mathbf{G} - \mathbf{N})\mathbf{T}, \tag{6}$$
$$\Lambda_2(\xi, u) \coloneqq \mathrm{ad}_{\boldsymbol{b}^\wedge}[\Pi(\Lambda_1(\xi, u))], \tag{7}$$
$$\Lambda_3(\xi, u) \coloneqq \boldsymbol{t}^\wedge \left({}^I\boldsymbol{\omega} - \boldsymbol{b}_{\boldsymbol{\omega}}\right), \tag{8}$$
$$\Lambda_4(\xi, u) \coloneqq \mathbf{S}^\top \left({}^I\boldsymbol{\omega} - \boldsymbol{b}_{\boldsymbol{\omega}}\right). \tag{9}$$

The map $\Lambda(\xi, u)$ is a lift for the system in Equ. (1) with respect to the symmetry group $\mathbf{G}$.

V. Equivariant Filter Design

The derivation of the linearized error dynamics, as well as linearized output, are defined according to [9], [13] for the case of equivariant output, that is:

$$\dot{\boldsymbol{\varepsilon}} \approx \mathbf{A}_t^0 \boldsymbol{\varepsilon} - \mathrm{D}_e|_{\mathring{\xi}} \vartheta(e)\, \mathrm{D}_E|_I \phi_{\mathring{\xi}}(E)[\Delta],$$
$$\mathbf{A}_t^0 = \mathrm{D}_e|_{\mathring{\xi}} \vartheta(e)\, \mathrm{D}_\xi|_{\hat{\xi}} \phi_{\hat{X}^{-1}}(\xi)\, \mathrm{D}_E|_I \phi_{\hat{\xi}}(E)$$
$$\mathrm{D}_\xi|_{\phi_{\hat{X}}(\mathring{\xi})} \Lambda(\xi, u)\, \mathrm{D}_e|_{\mathring{\xi}} \phi_{\hat{X}}(e)\, \mathrm{D}_{\boldsymbol{\varepsilon}}|_{\mathbf{0}} \vartheta^{-1}(\boldsymbol{\varepsilon}),$$
$$\delta(h(e)) = \delta\left(\rho_{\hat{X}^{-1}}(h(\xi))\right) \approx \mathbf{C}^\star \boldsymbol{\varepsilon} + \mathbf{O}(\varepsilon^3),$$
$$\mathbf{C}^\star \boldsymbol{\varepsilon} = \frac{1}{2} \mathrm{D}_y|_{\mathring{y}} \delta(y) \left(\mathrm{D}_E|_I \rho_E(\mathring{y}) + \mathrm{D}_E|_I \rho_E\left(\rho_{\hat{X}^{-1}}(y)\right)\right) \varepsilon^\wedge.$$

In this work, we choose the state origin to be the identity of the state space, thus $\mathring{\xi} = \mathrm{id}$, and we make use of normal coordinates introduced in [9]. Therefore, let $\mathbf{G}$ be the symmetry group, let $\phi_{\hat{X}^{-1}}(\xi)$ denote the equivariant error, then define normal coordinates $\boldsymbol{\varepsilon} = \vartheta(e) \coloneqq \log\left(\phi_{\mathring{\xi}}^{-1}(e)\right)^\vee \in \mathbb{R}^n$, where $\log : \mathbf{G} \to \mathfrak{g}$ is the logarithm of the symmetry group.

Let $\boldsymbol{\varepsilon} \in \mathbb{R}^{21}$, then the linearized error state matrix $\mathbf{A}_t^0 \mid \dot{\boldsymbol{\varepsilon}} \simeq \mathbf{A}_t^0 \boldsymbol{\varepsilon}$ is defined according to

$$\mathbf{A}_t^0 = \left[\begin{array}{cc:cc:cc} \multicolumn{2}{c:}{{}_1\mathbf{A}} & \multicolumn{2}{c:}{\mathbf{I}_6} & \mathbf{0}_{6\times3} & \mathbf{0}_{6\times3} \\ & & \hat{b}^\wedge & \mathbf{0}_{3\times3} & \mathbf{0}_{3\times3} & \mathbf{0}_{3\times3} \\ \hdashline \mathbf{0}_{6\times3} & \mathbf{0}_{6\times6} & \multicolumn{2}{c:}{{}_2\mathbf{A}} & \mathbf{0}_{6\times3} & \mathbf{0}_{6\times3} \\ \hdashline \mathbf{0}_{6\times3} & \mathbf{0}_{6\times6} & \mathbf{0}_{3\times3} & \mathbf{0}_{3\times3} & {}_3\mathbf{A} & \mathbf{0}_{3\times3} \\ \hdashline -{}_3\mathbf{A} & \mathbf{0}_{6\times6} & \mathbf{I}_3 & \mathbf{0}_{3\times3} & \mathbf{0}_{3\times3} & {}_3\mathbf{A} \end{array}\right], \tag{10}$$

where

$${}_1\mathbf{A} = \begin{bmatrix} \mathbf{0}_{3\times3} & \mathbf{0}_{3\times3} & \mathbf{0}_{3\times3} \\ {}^G\boldsymbol{g}^\wedge & \mathbf{0}_{3\times3} & \mathbf{0}_{3\times3} \\ \mathbf{0}_{3\times3} & \mathbf{I}_3 & \mathbf{0}_{3\times3} \end{bmatrix} \in \mathbb{R}^{9\times9},$$
$${}_2\mathbf{A} = \mathbf{ad}^\vee_{\left(\left(\Pi\left(\mathrm{Ad}_{\hat{C}}[\mathbf{W}] + \mathbf{G}\right) + \hat{\gamma}\right)^\vee\right)} \in \mathbb{R}^{6\times6}$$
$${}_3\mathbf{A} = \left(\hat{A}\,{}^I\boldsymbol{\omega} + \hat{\gamma}_\omega\right)^\wedge \in \mathbb{R}^{3\times3}.$$

Let y_m, y_p, y_v represent the raw measurements of direction, position, and velocity, respectively. Then, given the configuration output in Equ. (2, 3, 4), the actions on the output space defined in Tab. III, and the use of normal coordinates, the three linearized output matrices yield

$$\mathbf{C}_m^\star = {}^G\boldsymbol{m}^\wedge \begin{bmatrix} \mathbf{0}_{3\times15} & \frac{1}{2}\left({}^G\boldsymbol{m} + \hat{E} y_d\right)^\wedge & \mathbf{0}_{3\times3} \end{bmatrix}, \tag{11}$$
$$\mathbf{C}_p^\star = \begin{bmatrix} \frac{1}{2}\left(y_p + \hat{b} - \hat{d}\right)^\wedge & \mathbf{0}_{3\times3} & -\mathbf{I}_3 & \mathbf{0}_{3\times6} & \mathbf{I}_3 & \mathbf{0}_{3\times3} \end{bmatrix}, \tag{12}$$
$$\mathbf{C}_v^\star = \begin{bmatrix} \frac{1}{2}\left(y_v + \hat{a} - {}^I\boldsymbol{\omega}^\wedge \hat{d}\right)^\wedge & -\mathbf{I}_3 & \mathbf{0}_{3\times9} & {}^I\boldsymbol{\omega}^\wedge & \mathbf{0}_{3\times3} \end{bmatrix}. \tag{13}$$

VI. Uncertain observation handling

Uncertain observation and signal outages are particularly common in inertial navigation scenarios. typical solutions rely on χ^2 rejection tests. However, binary rejection strategies are often insufficient and very sensitive to tuning parameters. In the present subsection, we present the strategy for robust uncertain observation handling, based on the concept of generalized covariance union GCU [15], [16] for which tuning is a simple choice of convergence rate.

Let y represent an observation and $\mathbf{R}$ the observation covariance. Let $\mathbf{C}^\star$ represent the linearized output matrix, and $\boldsymbol{\Sigma}$ be the estimated state covariance. Let $\tilde{\boldsymbol{y}}$ be the innovation computed via the output action, and $\mathbf{S}$ be the innovation covariance. Let $\alpha \in [0, 1]$ be a scalar value used to control the convergence rate (the lower, the faster). Then, before updating the filter states according to [9], we compute an inflated innovation covariance $\mathbf{S}'$ as follows:

$$r = \tilde{\boldsymbol{y}}^\top \mathbf{S}^{-1} \tilde{\boldsymbol{y}} = \tilde{\boldsymbol{y}}^\top \left(\mathbf{C}^\star \boldsymbol{\Sigma} \mathbf{C}^{\star\top} + \mathbf{R}\right)^{-1} \tilde{\boldsymbol{y}},$$
$$\beta = \begin{cases} \frac{\left(1+\sqrt{r}\right)^2}{1+r} & \text{if } r < 1 \\ 2 & \text{otherwise} \end{cases},$$
$$\mathbf{S}' = \beta\left(\mathbf{C}^\star \boldsymbol{\Sigma} \mathbf{C}^{\star\top} + \alpha \tilde{\boldsymbol{y}} \tilde{\boldsymbol{y}}^\top\right) + \mathbf{R}.$$

The underlying idea is to inflate the innovation covariance in the direction of the innovation and in such a way that after the inflation the quantity $\tilde{\boldsymbol{y}}^\top \mathbf{S}'^{-1} \tilde{\boldsymbol{y}}$ is smaller than 1 [15], [16].

VII. Experiments

In the following subsections, we present and analyze various experiments conducted using both simulated data within the ArduPilot's software in the loop (SITL) environment and real-world flight data. These experiments aim to evaluate the performance of the proposed methodologies under challenging scenarios outlined in Sec. I. Each experiment includes a flying aircraft equipped with multiple IMUs, GNSS receivers, magnetometers, and other sensors such as barometers. The ArduPilot EKF3 was set to use any available sensor, whereas the proposed EqF is set to fuse the measurements from IMUs, GNSS receivers, and magnetometers. In each experiment, the ArduPilot EKF3 is set with accurate truth values for calibration states. In contrast, the EqF was initialized with zero GNSS lever arm and identity magnetometer rotational calibration – these states are self-calibrated online. Additionally, in all the experiments, the tuning parameters of the filters were left

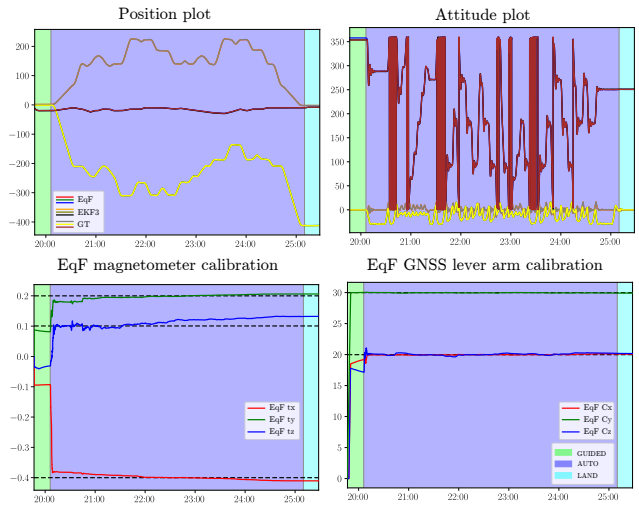

Figure 2. Comparison of the proposed EqF and the ArduPilot's EKF3 for a SITL quadcopter flight. **Top**, Position, and attitude estimates. **Bottom**, Estimation of GNSS lever arm ${}^{I}\boldsymbol{t}$ (left) and magnetometer rotational calibration ${}^{I}\mathbf{R}_{M}$ (right) using the proposed EqF. Dashed lines represent reference values, y-axes are in meters and degrees, x-axes in mm::ss format.

unchanged to their default values. For all experiments, we used original parameters provided by ArduPilot for both their SITL environment and EKF3. We refer the reader to the ArduPilot documentation for the complete set of values. The proposed EqF was set with a similar but less inflated selection of default parameters that were found to work well in practice.

A. SITL: software in the loop simulations

In the SITL environment, we conducted three distinct experiments. The first experiment was targeted at showing the self-calibration capabilities of the proposed EqF. To achieve this, we simulated a quadcopter with magnetometer rotational calibrations at angles of $20°$, $30°$, and $20°$, along with a GNSS lever arm of -0.4m, 0.2m, 0.1m in the xyz axes, respectively. The outcomes, depicted in Fig. 2, show the estimated positions and attitudes generated by both, the proposed EqF and the ArduPilot's EKF3. Additionally, the estimated sensor extrinsic calibration by the equivariant filter is illustrated. The results indicate that while both filters generally exhibit good performance, the EqF achieves effective estimation of all the states, including the sensor's extrinsic parameters, without prior knowledge of these parameters.

The second experiment was targeted at showing the consistent nature of the proposed EqF under static conditions. EKFs suffer from spurious information gains when receiving position updates under constant velocity or static conditions, leading to what is commonly termed as *false observability* [8]. Results in Fig. 3 highlight the behavior of the proposed EqF and the ArduPilot's EKF3 in a prolonged simulated static scenario. In this scenario, the EqF achieves zero error in position and a constant error in attitude, mainly due to the initial yaw estimate of $0°$, whereas the actual yaw is approximately $7°$. On the contrary, the EKF3 displays the classical symptoms of the false observability problem. It incorrectly gains spurious information, resulting in an erroneous and non-constant estimation of

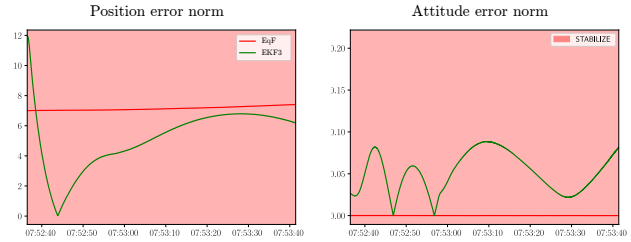

Figure 3. Position error norm (left) and attitude error norm (right) using the proposed EqF and the ArduPilot's EKF3 in a simulated static scenario. The EKF3 exhibits a wrong estimate, showing the typical symptoms of inconsistency due to false observability in static conditions. On the contrary, the proposed EqF achieves a consistent estimate.

the yaw. Constant velocity motion and static conditions are common scenarios in autonomous missions, and hence, the ability to handle such situations without the need for exception code is of paramount importance.

The final experiment in the SITL environment is targeted at evaluating the behavior of the filters in the presence of GNSS signal outages. In particular, we analyze the gating system of the ArduPilot's EKF3, and the inflation strategy discussed in Sec. VI and applied to the proposed EqF. Fig. 4 shows that both filters are unaffected by GNSS glitches and keep providing a good estimate (the EKF3 due to code modules for exception-handling, our EqF inherently due to the proposed innovation-covariance inflation). Furthermore, Fig. 4 shows the behavior of the EKF3 and the EqF on a scenario where a GNSS shift happens. The ArduPilot's EKF3 jumps to the new solution after 10s a shift is observed due to exception code. The conditions for the jump include outlier rejection identification criteria, the period to wait before resetting the state, and modifications for the covariance during the period that the outliers are rejected. In contrast, the EqF behavior is dependent only on the parameter α that governs the inflation rate. The transition can be tuned to perform a smooth transition or a semi-smooth transition. The flexibility of the proposed EqF allows it to work properly with different controller implementations.

B. SpringValley: outdoor quadcopter flight

In this subsequent experiment, real-world flight data from a quadcopter was collected to validate the previously discussed results in the software in the loop simulation environment. Due to the absence of ground truth data, our analysis focuses on the position and velocity error norms in relation to the measurements obtained from a real time kinematics (RTK) GNSS. The error plots in Fig. 5 depict a comparison between the proposed EqF and the ArduPilot's EKF3. Notably, the EqF achieves lower error compared to the EKF3.

C. BraveHeart: outdoor quadcopter flight with faulty IMU

In this concluding experiment, we evaluate the ability of the filters to handle a faulty IMU afflicted by high amplitude, high-frequency components, potentially stemming from excessive vibrations and aliasing effects. An illustration of this scenario is presented in Fig. 6, showing the low-passed filtered signal

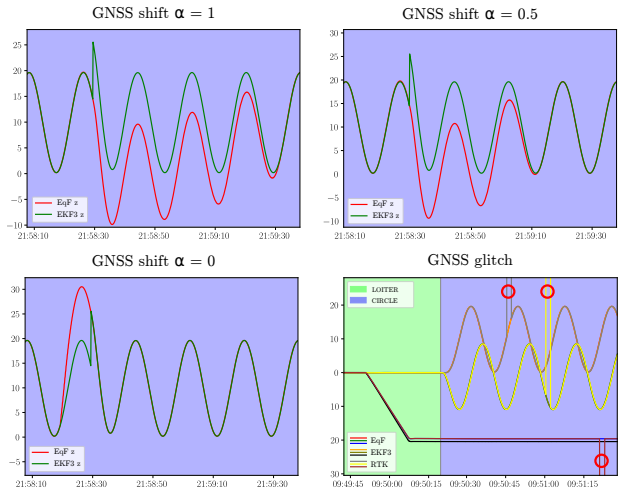

Figure 4. Behavior of the ArduPilot's EKF3 and the proposed EqF in case of GNSS shifts. The plots show the behavior of the filters following a GNSS shift happening at $22:58:20$. **Top left**, smooth transition of the proposed EqF implementing the strategy discussed in Sec. VI with $\alpha = 1$. **Top right**, semi-smooth transition of the proposed EqF implementing the strategy discussed in Sec. VI with $\alpha = 0.5$. **Bottom left**, transition with $\alpha = 1.0$. **Bottom right**, behavior of the ArduPilot's EKF3 and the proposed EqF in case of multiple GNSS glitches highlighted with red circles.

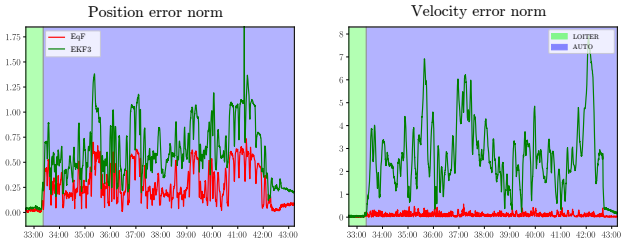

Figure 5. Position and velocity estimation error when compared to raw RTK GNSS measurements, using the proposed EqF and the ArduPilot's EKF3 on a real world quadcopter flight.

from two accelerometers recorded from an actual quadcopter flight. The accelerometer from IMU[0] is faulty and exhibits substantial high-frequency artifacts, setting it apart from the healthy IMU[1].

In this experiment, we demonstrate the superior robustness of the proposed EqF. It effectively provides an accurate estimate when used with the faulty IMU, eliminating the need for specialized parameter adjustments. In particular, we compare the EqF run with the faulty IMU and with standard tuning parameters with two instances of the ArduPilot's EKF3, one with the faulty IMU, and the second one with the healthy IMU. Fig. 6 shows that the EqF succeeds in providing an accurate estimate when paired with the faulty IMU while the EKF3 encounters challenges, only succeeding under specific tuning conditions involving high process noise and reduced observation noise.

VIII. Conclusion

In this study, we introduced a new EqF design and implementation: We derived a multi-sensor fusion algorithm with

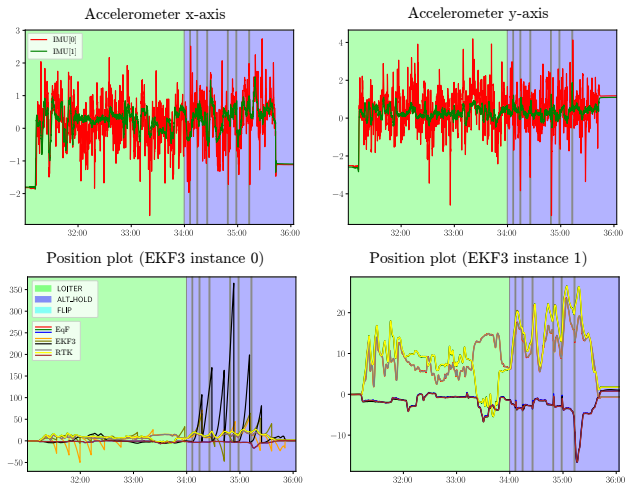

Figure 6. Performance comparison of the proposed EqF and the EKF3 receiving measurements from two different IMUs, one of which is faulty. On the **top**, the low-pass filtered acceleration along the x (left) and y (right) axes for two IMUs. It is observed that IMU[0] (in red) is faulty and suffers from high amplitude components at high frequency, while IMU[1] (in green) is healthy. On the **bottom left**, the plot shows the estimates obtained from both the proposed EqF and an instance of the ArduPilot's EKF3 when used with measurements from the faulty IMU. The **bottom right** plot compares the estimate from the proposed EqF when used with measurements from the *faulty* IMU and a second instance of the ArduPilot's EKF3 that relies on measurements from the *healthy* IMU. The EKF3 fails to provide accurate estimation when dealing with data from the faulty IMU, while the proposed EqF demonstrates superior robustness by effectively dealing with it.

self-calibration capabilities, extending the previously introduced Semi-Direct-Bias symmetry group [13] with velocity measurements and effectively incorporating extrinsic calibration parameters for GNSS receivers and magnetometers. Our formulation achieves third-order linearization error of the output map leading to improved estimation performance. Through a series of experiments conducted in both the software in the loop simulation environment and real-world scenarios, we demonstrated that the proposed EqF provides an effective solution to challenging scenarios encountered in UAV operations.

The proposed algorithm achieves consistent and good estimation results requiring minimal parameter tuning and no knowledge about the sensors' extrinsic parameters. Even when used with noisy and faulty IMUs, the proposed solution achieves remarkable robustness. Furthermore, in case of measurement shift, the implemented innovation covariance inflation strategy allows for different behaviors to be set, making the proposed EqF a flexible solution for different controller implementations.

Future work includes the extension to other sensor modalities available to commercial UAV such as barometer and optical flow sensors.

Acknowledgement

The authors would like to thank the Ardupilot community for access to flight data logs and Paul Riseborough for insight into the Ardupilot EKF INS solution.

REFERENCES

[1] S. J. Julier, J. K. Uhlmann, and H. F. Durrant-Whyte, "New approach for filtering nonlinear systems," *Proceedings of the American Control Conference*, vol. 3, pp. 1628–1632, 1995.

[2] G. P. Huang, A. I. Mourikis, and S. I. Roumeliotis, "A first-estimates Jacobian EKF for improving SLAM consistency," in *Experimental Robotics: The Eleventh International Symposium*. Springer, 2009, pp. 373–382.

[3] J. A. Hesch, D. G. Kottas, S. L. Bowman, and S. I. Roumeliotis, "Consistency analysis and improvement of vision-aided inertial navigation," *IEEE Transactions on Robotics*, vol. 30, no. 1, pp. 158–176, 2014.

[4] W. Xu and F. Zhang, "FAST-LIO: A Fast, Robust LiDAR-inertial odometry package by tightly-coupled iterated kalman filter," *IEEE Robotics and Automation Letters*, vol. 6, no. 2, pp. 3317–3324, 4 2021.

[5] J. Preiss, K. Hausman, G. S. Sukhatme, and S. Weiss, "Simultaneous self-calibration and navigation using trajectory optimization," *The International Journal of Robotics Research*, vol. 37, no. 13-14, pp. 1573–1594, 2018.

[6] L. Meier, D. Honegger, and M. Pollefeys, "PX4: A Node-Based Multithreaded Open Source Robotics Framework for Deeply Embedded Platforms," in *2015 IEEE International Conference on Robotics and Automation (ICRA)*. Seattle, Washington, USA: IEEE, 5 2015, pp. 6235–6240. [Online]. Available: http://ieeexplore.ieee.org/document/7140074/

[7] "ArduPilot." [Online]. Available: https://ardupilot.org/

[8] A. Barrau and A. Barrau, "Non-linear state error based extended Kalman filters with applications to navigation," Ph.D. dissertation, Mines Paristech, 9 2015. [Online]. Available: https://hal.archives-ouvertes.fr/tel-01247723

[9] P. van Goor, T. Hamel, and R. Mahony, "Equivariant Filter (EqF)," *IEEE Transactions on Automatic Control*, 6 2022.

[10] E. J. Lefferts, F. L. Markley, and M. D. Shuster, "Kalman Filtering for Spacecraft Attitude Estimation," *https://doi.org/10.2514/3.56190*, vol. 5, no. 5, pp. 417–429, 5 1982. [Online]. Available: https://arc.aiaa.org/doi/10.2514/3.56190

[11] A. Fornasier, Y. Ng, R. Mahony, and S. Weiss, "Equivariant Filter Design for Inertial Navigation Systems with Input Measurement Biases," *2022 International Conference on Robotics and Automation (ICRA)*, pp. 4333–4339, 5 2022. [Online]. Available: https://ieeexplore.ieee.org/document/9811778/

[12] A. Fornasier, Y. Ng, C. Brommer, C. Bohm, R. Mahony, and S. Weiss, "Overcoming Bias: Equivariant Filter Design for Biased Attitude Estimation With Online Calibration," *IEEE Robotics and Automation Letters*, vol. 7, no. 4, pp. 12 118–12 125, 10 2022.

[13] A. Fornasier, Y. Ge, P. van Goor, R. Mahony, and S. Weiss, "Equivariant Symmetries for Inertial Navigation Systems," *arXiv preprint arXiv:2309.03765*, 9 2023. [Online]. Available: https://arxiv.org/abs/2309.03765v1

[14] M. Scheiber, A. Fornasier, C. Brommer, and S. Weiss, "Revisiting Multi-GNSS Navigation for UAVs – An Equivariant Filtering Approach," *2023 21st International Conference on Advanced Robotics (ICAR)*, pp. 134–141, 12 2023. [Online]. Available: https://ieeexplore.ieee.org/document/10406552/

[15] S. Reece and S. Roberts, "Generalised covariance union: a unified approach to hypothesis merging in tracking," *IEEE Transactions on Aerospace and Electronic Systems*, vol. 46, no. 1, pp. 207–221, 1 2010.

[16] M. Ghobadi, P. Singla, and E. T. Esfahani, "Robust attitude estimation from uncertain observations of inertial sensors using covariance inflated multiplicative extended kalman filter," *IEEE Transactions on Instrumentation and Measurement*, vol. 67, no. 1, pp. 209–217, 1 2018.

[17] R. Mahony, T. Hamel, and J. Trumpf, "Equivariant Systems Theory and Observer Design," *arXiv preprint arXiv:2006.08276*, 6 2020. [Online]. Available: https://arxiv.org/abs/2006.08276v3